ITERATIVE RECONSTRUCTION FOR X-RAY DARK FIELD IMAGING CT: ARTIFACTS REDUCTION FOR HARD AND SOFT MIXTURE TISSUE

Naoki Sunaguchi,[1] Tetsuya Yuasa,[2] Masami Ando[3]
[1]Institution Faculty of Science and Technology, Gunma University, Kiryu, Gunma 376-8515, Japan
[2]Graduate School of Science and Engineering, Yamagata University, Yonezawa, Yamagata 992-8510, Japan
[3]Research Institute for Science and Technology, Tokyo University of Science, Noda, Chiba 278-8510, Japan
E-mail: sunaguchi@gunma-u.ac.jp

ABSTRACT
Phase-contrast x-ray CT using refraction angle analyzer crystal can delineate biological soft tissues in a much higher contrast than that of conventional absorption-contrast CT. However, if an object includes bones or calcified tissues region, they generate radial artifacts similar to the metal artifacts occurring in clinical CT because their refraction-indices are much higher than those of soft tissues, leading to impaired observation. In order to well observe an object composed of bones or calcified tissues and soft tissues, the artifacts should be removed. In this research, we propose a reconstruction algorithm for analyzer-based phase-contrast computed tomography (CT) applicable to biological samples including hard tissues. The algorithm is an iterative procedure that goes back and forth between a tomogram and its sinogram through the Radon transform and CT reconstruction while imposing a priori information in individual regions. We demonstrate the efficacy of the algorithm using synthetic data generated by computer simulation reflecting actual experimental conditions and actual data acquired from a foot of rat including rheumatoid arthritis by a dark field imaging system.

KEY WORDS
Iterative reconstruction algorithm, analyzer-based phase-contrast CT, refractive index, computed tomography, synchrotron x ray, DEI, x-ray dark-field imaging.

1. Introduction

Angular analyzer based phase-contrast CT imaging such as DEI (diffraction enhanced imaging) [1] or DFI (dark field imaging) [2] estimates projections for absorption- and refraction-contrast CT from the two sets of measured transmitted intensities containing both absorption and refraction information using the rocking curve(s) of the analyzer [3-5]. A refraction-contrast CT image is reconstructed from the estimated differential refraction projections by convolving them with a signum function, i.e., $\mathrm{sgn}(\xi) = 1$ for $\xi \geq 0$, -1 for $\xi < 0$, and then applying a filtered back projection (FBP) method [6]; an absorption-contrast CT image is reconstructed from the absorption projections by directly applying the FBP method. Thus, phase-contrast CT can reproduce a three-dimensional distribution of refractive indices in biological soft tissue with high contrast and that of linear absorption coefficients, and provide new information on biological soft tissues, e.g., breast cancer tissues, with respect to pathology and physiology [7-9]. However, in a case that a sample includes hard tissues, e.g., calcification or bone, radial artifacts may appear throughout a refraction-contrast CT image, while an absorption-contrast CT may clearly depict only hard tissue regions. This is because the estimation of refraction projections with the rocking curve(s) fails; x-ray flux impinging on hard-tissue regions with relatively higher refractive index decrement δ at a large incident angle deviate from the measurable region in the rocking curve(s). The artifacts impair extraction of useful information on a biological sample from the reconstructed image.

In this study, we devise an algorithm to reduce artifacts in a reconstructed image and restore the image quality. Here, we treat the refraction projection data for x-ray flux impinging on hard tissue regions at a large incident angle as missing data. Under the condition, the proposed algorithm iteratively goes back and forth between a refraction-contrast tomogram and its sinogram while imposing a priori information on both the tomogram and sinogram. In order to demonstrate the effectiveness, we compare the results by the conventional method with ones by the proposed algorithm for the data obtained from computer simulation and experiment.

2. Reconstruction algorithm

The proposed algorithm is an iterative procedure in which it goes back and forth between a refraction-contrast tomogram and its sinogram through a Radon transform and CT reconstruction while imposing a priori information on both the tomogram and sinogram. It requires a set of absorption projections obtained from direct transmission without an analyzer and a set of projections containing absorption and refraction information acquired with an angular analyzer. The reason for the required absorption projections is that both absorption and refraction information is not available at the same time for x-ray flux impinging on hard tissue regions at a large incident angle when acquisition of two sets of projections is required.

DOI: 10.2316/J.2014.216.818-0030

The reconstruction begins with the following preprocessing. First, we separate differential refraction projections using the measured absorption projections from the measured projections containing both absorption and refraction information to obtain a refraction sinogram $p^{(0)}(\xi,\theta)$. Next, we reconstruct an absorption-contrast tomogram from the measured absorption projections to specify hard tissue regions. Subsequently, for each projection angle θ we specify missing-data regions in a differential refraction projection R_θ by finding x-ray flux impinging on hard tissue regions at a large incident angle according to the imaging geometry using the absorption-contrast tomogram; that is, we specify the missing-data region R_θ in the differential refraction projection $p^{(0)}(\xi,\theta)$ for each θ. Finally, we specify the object region S from the refraction-contrast tomogram reconstructed with the conventional algorithm (Figure 1).

Provided $p^{(0)}(\xi,\theta)$, R_θ, and S, the algorithm is as follows:

Step1: Feed an initial refraction tomogram $f^{(1)}(x,y)$, reconstructed with the conventional method [6] and then smoothed to maximally reduce artifacts, and set $n = 1$.

Step2: Transform a tomogram updated n times, $f^{(n)}(x,y)$, to the sinogram, $p^{(n)}(\xi,\theta)$, for each θ by performing line-integrals along each x-ray flux according to the imaging geometry (i.e., the Radon transform) and then differentiate them with respect to ξ, where ξ is an axis perpendicular to a direction of the x-ray flux (Figure 1), that is,

$$p^{(n)}(\xi,\theta) = \partial/\partial\xi \left(\Re_\theta f^{(n)}\right)(\xi,\theta), \qquad (1)$$

where $\Re_\theta$ is a projection operator for θ.

Step3: First, replace the data in the region except the missing-data region, $\overline{R}_\theta$, with the corresponding data in $p^{(0)}(\xi,\theta)$. Next, impose to the differential refraction projections the condition that the total sum of the differential projection should be zero for each θ in terms of the following mathematical fact: Consider a general smooth function $\phi(u)$ with $\lim_{|u|\to\infty}\phi(u) = 0$. Since $\phi(-\infty) = 0$ from the precondition,

$$\int_{-\infty}^{v} \frac{d\phi}{du} du = \phi(v) - \phi(-\infty) = \phi(v). \qquad (2)$$

Therefore, $\int_{-\infty}^{\infty} \frac{d\phi}{du} du = 0$, because $\phi(\infty) = 0$. From the mathematical theorem, since the Radon transform of $f(x,y)$ with a support, $(\Re_\theta f)(\xi,\theta)$, always satisfies $\lim_{|\xi|\to\infty}(\Re_\theta f)(\xi,\theta) = 0$,

$$\int_{-\infty}^{\infty} p(\xi,\theta) d\xi = \int_{-\infty}^{\infty} \frac{\partial}{\partial\xi}(\Re_\theta f)(\xi,\theta) d\xi = 0 \qquad (3)$$

for each θ. Thus, the total sum of the differential projection should be zero for each θ.

We straightforwardly use the original projection data obtained from measurement $p^{(0)}(\xi,\theta)$ in regions $\overline{R}_\theta$ except the missing-data region R_θ. And, we replace the data in the missing-data region R_θ with the data obtained at the nth iteration $p^{(n)}(\xi,\theta)$. However, the straightforward use of $p^{(n)}(\xi,\theta)$ in the missing-data R_θ will violate Eq. (3). Therefore, we should modify the data in the missing-data region. We propose the update rule as follows:
for each θ,

$$\tilde{p}^{(n)}(\xi,\theta) = \begin{cases} p^{(0)}(\xi,\theta) & \text{for } \xi \in \overline{R}_\theta \\ k\, p^{(n)}(\xi,\theta) & \text{for } \xi \in R_\theta \end{cases}, \qquad (4)$$

where k satisfies

$$\int_{\overline{R}_\theta} p^{(0)}(\xi,\theta) d\xi + k\int_{R_\theta} p^{(n)}(\xi,\theta) d\xi = 0, \qquad (5)$$

because $\int_{-\infty}^{\infty} \tilde{p}^{(n)}(\xi,\theta) d\xi = 0$ should hold from Eq. (3).

Step4: Transform the updated refraction sinogram, $\tilde{p}^{(n)}(\xi,\theta)$, to the tomogram, $\tilde{f}^{(n)}(x,y)$, by convolving it with the signum function for each θ and then applying FBP; that is,

$$\tilde{f}^{(n)}(x,y) = (\Im(\mathrm{sgn}\otimes\tilde{p}^{(n)}))(x,y), \qquad (6)$$

where $\Im$ is a reconstruction operator for converting from the sinogram to the tomogram using FBP.

Step5: Replace the pixel value in the region except the object region S, $\overline{S}$ with zero, and set $n = n + 1$; that is,

$$f^{(n+1)}(x,y) = \begin{cases} \tilde{f}^{(n)}(x,y) & \text{for } (x,y) \in S \\ 0 & \text{for } (x,y) \in \overline{S} \end{cases}. \qquad (7)$$

Step6: Iterate Steps 2 through 5 until $\left\| f^{(n+1)}(x,y) - f^{(n)}(x,y) \right\| / \left\| f^{(n)}(x,y) \right\|$ converges to the predefined value (e.g., 1.0×10^{-3})

The proposed algorithm as illustrated in Figure 2 is similar to Papoulis's algorithm to extrapolate a signal from the band-limited condition [10] and Fienup's algorithm to retrieve phase information from an intensity signal [11]. These are iterative algorithms that go back and forth between the signal and Fourier spaces through Fourier and inverse-Fourier transforms, while imposing a priori information on individual spaces. Considering that the sinogram has a one-to-one correspondence with the two-dimensional (2D) Fourier space through the Fourier slice theorem [12], the proposed algorithm may be regarded as their variation.

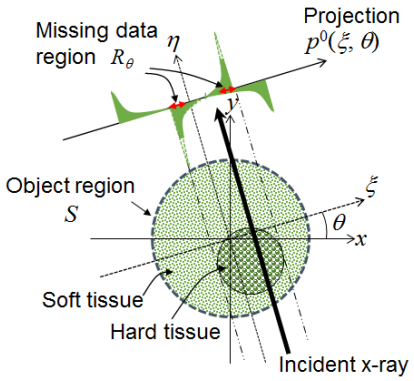

Figure 1. Imaging geometry.

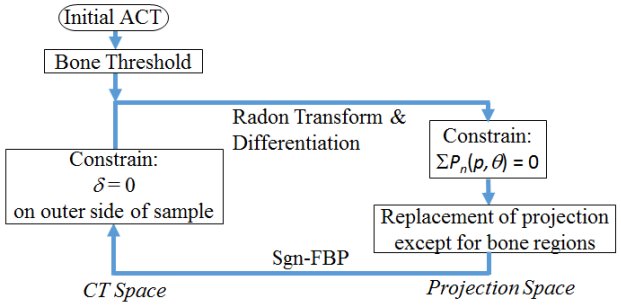

Figure 2. Block diagram of the proposed algorithm.

3. X-ray dark-field imaging (DFI) system

The efficacy of the algorithm is shown by applying it to synthetic and actual data from phase-contrast CT based on DFI. The schematic of DFI system is shown in Figure 3. The imaging system comprises an x-ray source, monochromator-collimator, an angular analyzer (AA), and an x-ray CCD camera. As the x-ray source, synchrotron x-ray has the vertically polarization in the beamline BL14C on a 2.5-GeV storage ring (KEK Photon Factory, Tsukuba, Japan), is used. MC is a Si (440) Bragg case crystal whose asymmetrical angle is 10.2°. AA is a Si (440) symmetric Laue case crystal whose thickness is approximately 150 μm. The thickness of AA is selected such that forward diffraction intensity becomes theoretically zero when an incident angle corresponds with its Bragg angle, i.e., dark field condition [2]. The Bragg angles of the both Si (440) crystals are 10.69°. The sample is placed between MC and AA. CCD camera, manufactured by Photonics Science, has with matrix size of 4864×3246, pixel size of 7.4×7.4 μm^2, a field of view of 36.1×24.0 mm^2, and 12-bit dynamic range. After white x-rays from the storage ring are monochromated by a double crystal monochromator to x-rays of 35 keV, the monochromated x-rays are further collimated and expanded into a volumetric parallel beam by the MC and incident on a sample (the number of photons just before a sample is 10^8 photons/mm^2). Each ray is refracted and simultaneously absorbed according to the refractive index and linear attenuation coefficient distributions of a sample, respectively. The transmitted beam impinges on AA, which produces two directional beams, i.e., forward diffraction and diffraction beams. Forward diffraction beams, whose intensities are modified according to the corresponding the rocking curve, are acquired by the CCD camera.

Using the DFI system, two sets of projections are acquired as follows: one set of projections, which include both absorption and refraction information, is at the angular position in the monotonically increasing region of the rocking curve, and the other set of projections, which include only absorption information, is at the angular position in the flat region of the rocking curve. Projections for refraction-contrast CT are estimated from the two sets of measured transmitted intensities containing both absorption and refraction information using the rocking curve of the analyzer [5].

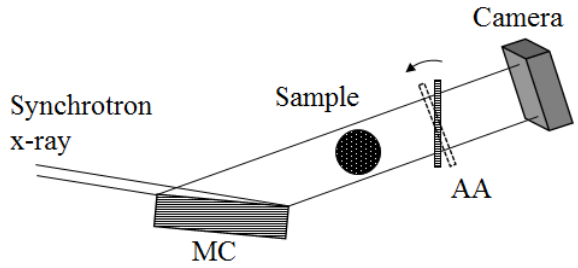

Figure 3. Schematics of dark-field imaging optics.

4. Simulation results

First, in order to evaluate the effectiveness of the proposed algorithm, the simulation experiment was carried out in an x-ray tracing manner based on geometrical optics which reflects actual physical parameters. Each ray was refracted at boundaries according to Snell's law, and simultaneously attenuated in a sample along the propagation path according to Beer's law. The rocking curve of the forward diffraction was calculated using the same parameters as those of the actual system based on dynamical diffraction theory. The simulator generated two distinct sets of projections: absorption and forward diffraction. With the help of the rocking curve, differential refraction projections were estimated from the two distinct sets of projections. The simulation used a numerical phantom consisting of a 6.3-mm diameter cylinder emulating soft tissue including multiple 0.9-mm diameter cylinders emulating hard tissue (Figure 4). Linear absorption coefficient and refractive index decrements of soft tissue were 3.6×10^{-1} cm^{-1} and 2.6×10^{-7}, respectively; those of hard tissues were 3.5×10^{0} cm^{-1} and 4.3×10^{-7}, respectively. Nine hundred projections were generated by rotating the phantom with a step size of 0.2° over 180°. Figure 5 (a) shows the absorption-contrast CT image reconstructed by the FBP method with a Shepp-Logan filter, in which only hard

tissues are clearly delineated. Figure 5 (b) shows the phase-contrast CT image reconstructed by the conventional method [6], in which conspicuous artifacts are observed throughout the whole image. Figure 5 (c) shows the phase-contrast CT image by the proposed method after the 4th iterations. The line profiles in Figure 6 plot the refractive index along the blue line indicated in Figure 5 (c), where the blue and red lines represent a theoretical value and a reconstructed value, respectively. It can be seen that the proposed algorithm operates satisfactorily, while the reconstructed values are slightly lower than the theoretical values in the soft tissue regions. Figure 7 shows the convergence properties of the algorithm, where the horizontal line is the iteration number and the vertical lines are the relative norm (RN) between the nth and (n+1)th tomograms (blue line) and the root mean square (RMS) between the nth and true tomograms (red line). RN and RMS are defined as below:

$$RN = \frac{\left\| f^{(n+1)}(x,y) - f^{(n)}(x,y) \right\|}{\left\| f^{(n)}(x,y) \right\|}, \text{ and} \qquad (8)$$

$$RMS = \sqrt{\frac{\left\| f^{n}(x,y) - f_{true}(x,y) \right\|^2}{N}}, \qquad (9)$$

where $f_{true}(x,y)$ and N are an image of the numerical phantom and number of pixels, respectively. It is observed that they both converge at the 4th iteration.

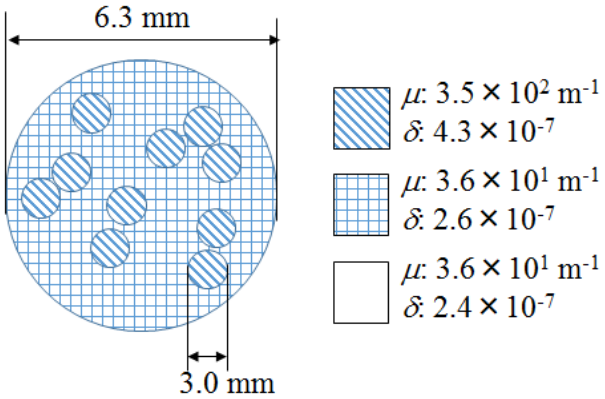

Figure 4. Schematics of a numerical phantom.

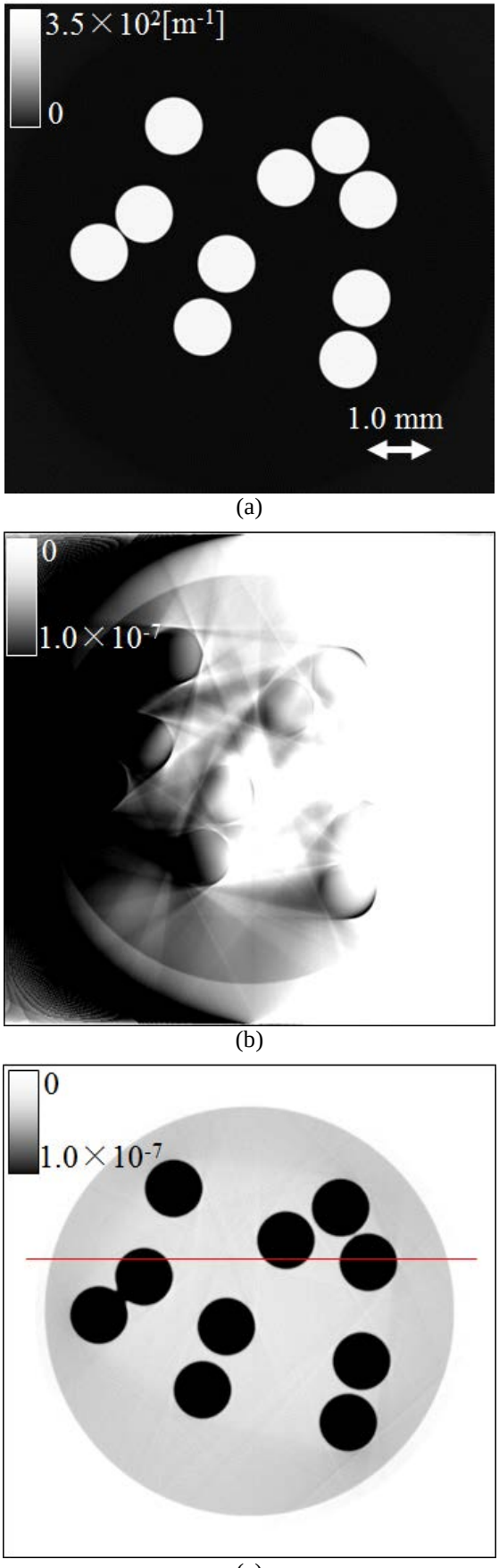

Figure 5. Reconstructed images of a numerical phantom. Absorption-contrast (a), phase-contrast by conventional method and phase contrast by proposed method.

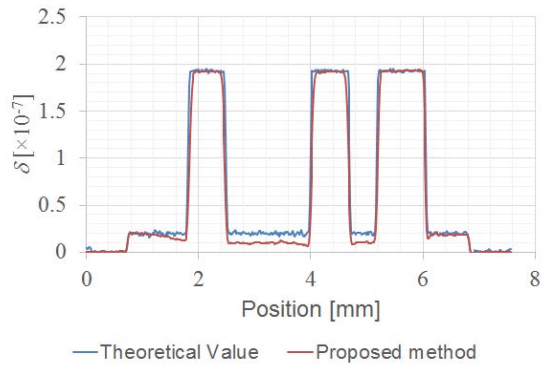

Figure 6. Plots of the refractive index vs. position of red line drawn in Figure 5 (c).

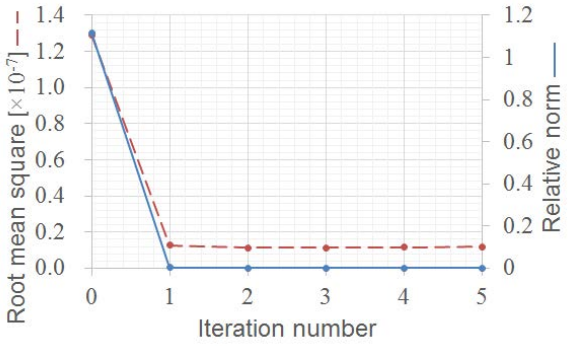

Figure 7. Convergence properties of the algorithm. Vertical axes of left and right are root mean square and relative norm, respectively.

5. Images of rat's foot with rheumatoid arthritis

We also applied the algorithm to a female Lewis rat's left hind foot in which rheumatoid arthritis was artificially developed by administering adjuvant at its right hind foot. Adjuvant used in this experiment was heat-killed Mycobacterium tuberculosis H37Ra cells (Difco Labs., Detroit, MI, USA) that had been emulsified with liquid paraffin (Wako Pure Chemical Industries, Osaka, Japan). It was amputated 21 days after the administration and fixed in a plastic tube filled with agarose gel. All procedures using the rat were in accordance with the "Guidelines for Animal Experimentation of the Japanese Association for Laboratory Animal Science," and were approved by the Animal Use and Care Committee at Mercian Cleantec Corporation. The sample is suitable to show the effectiveness of the proposed method because it is a mixture of low-density bones destructed by rheumatoid and high-density healthy bones. It is important for biomedical use to visualize such a complex tissue at high contrast. The sample size was approximately 23×23×35 mm^3. 900 projections of absorption and forward diffraction were acquired by rotating the sample with a step size of 0.2° over 180°. The total measurement time was about 2 hr. The differential refraction projections were estimated using the absorption projections. Figure 8 shows the maximum intensity projection (MIP) images of the absorption-contrast (a), phase-contrast by conventional method (b), and phase-contrast by proposed method (c), respectively. As can be clearly seen in Figure 8 (a), the absorption image shows only bone structures. Bone structure around the joints show black or dark colors. It shows that these areas are destroyed by rheumatoid arthritis. On the other hand, the phase-contrast images (Figure 8 (b) and (c)) show a lot of detailed structures inside the destructed bone shown as arrow *A* and skin outside bone structures. However, the artifacts and the lack of information due to them are observed in the bone and the joint regions as indicated by arrows *B* and *C* in Figure 8 (b). The phenomena are caused by the fact that the refraction-index of bone is much larger than that of soft tissue. As can be seen in Figure 8 (c), these deteriorations are dramatically improved by the proposed algorithm with the 3rd iteration. Especially, the destroyed bone regions indicated by arrow *A'* are clearly delineated, compared with those in Figure 8 (b). Also, the skin surface regions indicated by arrow *B'* in Figure 8 (c) are depicted at a high contrast, although the corresponding regions are contaminated with artifacts due to bone in Figure 8 (b). In addition, the invisible destroyed bone regions indicated by arrow *C* in Figure 8 (b) are restored in Figure 8 (c).

(a)

(b)

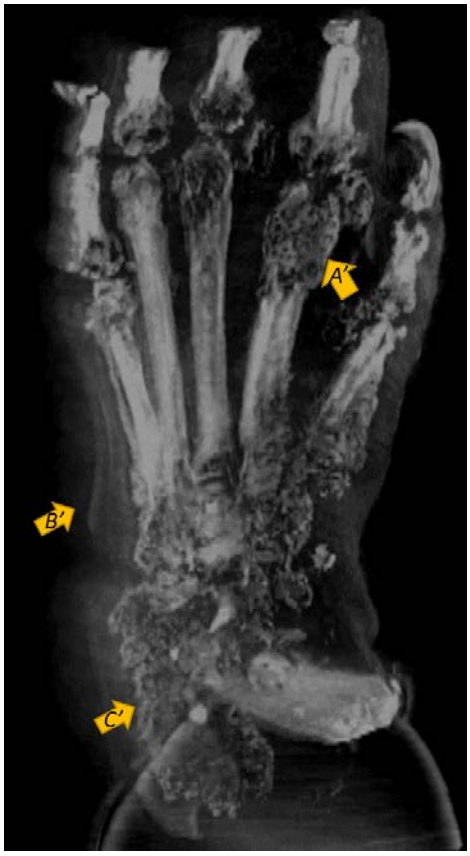

(c)

Figure 8. Reconstructed MIP images of a female Lewis rat's left hind foot with rheumatoid arthritis. (a) absorption-contrast, (b) phase-contrast by conventional method, and (c) phase-contrast by the proposed method.

6. Conclusion

The conventional reconstruction method for the phase-contrast CT has been very difficult to apply to samples including high refraction-index tissues such as bone or calcification in which the refraction saturation artifacts is generated. In order to remove these artifacts, the iterative algorithm with priori information is proposed. The proposed method demonstrates the superior capability of soft tissue recovery from the results of the simulation and the experiment of rat's foot in which rheumatoid arthritis. In future, it might be necessary for diagnosis of human body based on phase-contrast.

Acknowledgements

This research was partially supported by a Grant-In-Aid for Scientific Research (#20500385, #23602002, #24.1109) from the Japanese Ministry of Education, Science and Culture. This work was also supported (in part) by Grant for Basic Science Research Projects from The Sumitomo Foundation, JGC-S SCHOLARSHIP FOUNDATION, and Yazaki Memorial Foundation for Science and Technology. The experiment was performed under the approval of the PF User Association (PF-UA) at KEK under no. 2008S2002, 2011G672, and 2012G002 for use of the Photon Factory.

References

[1] D. Chapman, W. Thomlinson, R. E. Johnston, D. Washburn, E. Pisano, N. Gmur, Z. Zhong, R. Menk, F. Arfelli, & D. Sayers, Diffraction enhanced x-ray imaging, *Phys. Med. Biol.*, *42*(11), 1997, 2015-2025.

[2] M. Ando, A. Maksimenko, H. Sugiyama, W. Pattanasiriwisawa, K. Hyodo & C. Uyama, Simple X-Ray Dark- and Bright-Field Imaging Using Achromatic Laue Optics, *Jpn. J. Appl. Phys.*, *41*, 2002, L1016-L1018.

[3] F. A. Dilmanian, Z. Zhong, B. Ren, X. Y. Wu, D. Chapman, I. Orion & W. C. Thomlinson, Computed tomography of x-ray index of refraction using the diffraction enhanced imaging method, *Phys. Med. Biol.*, *45*(4), 2000, 933-946.

[4] A. Maksimenko, M. Ando, H. Sugiyama & T. Yuasa, Computed tomographic reconstruction based on x-ray refraction contrast, *Appl. Phys. Lett.*, *86*(12), 2005, 124105.

[5] N. Sunaguchi, T. Yuasa, Q. Huo, S. Ichihara & M. Ando, Convolution reconstruction algorithm for refraction-contrast computed tomography using a Laue-

case analyzer for dark-field imaging, *Appl. Phys. Lett.*, *97*(15), 2010, 153701.
[6] N. Sunaguchi, T. Yuasa, Q. Huo & M. Ando, Convolution reconstruction algorithm for refraction-contrast computed tomography using a Laue-case analyzer for dark-field imaging, *Opt. Lett.*, *36*(3), 2011, 391-393.
[7] S. Ichihara, M. Ando, A. Maksimenko, T. Yuasa, H. Sugiyama, E. Hashimoto, K. Yamasaki, K. Mori, Y. Arai, & T. Endo, 3-D reconstruction and virtual ductoscopy of high-grade ductal carcinoma in situ of the breast with casting type calcifications using refraction-based X-ray CT, *Virchows Arch*, *452*(1), 2008, 41-47.
[8] Y. Zhao, E. Brun, P. Coan, Z. Huang, A. Sztrókay, P. C. Diemoz, S. Liebhardt, A. Mittone, S. Gasilov, J. Miao & A. Bravin, High-resolution, low-dose phase contrast X-ray tomography for 3D diagnosis of human breast cancers, *PNAS*, *109*(45), 2012, 18290-18294.
[9] M. Ando, N. Sunaguchi, Yanlin Wu, Synho Do, Yongjin Sung, Abner Louissaint, Tetsuya Yuasa, Shu Ichihara & Rajiv Gupta, Crystal analyser-based X-ray phase contrast imaging in the dark field: implementation and evaluation using excised tissue specimens, *Eur. Radiol.*, *24*(2), 2014, 423-433.
[10] A. Papoulis, A new algorithm in spectral analysis and band-limited extrapolation, *IEEE Trans. Circuits and Systems*, *22*(9), 1975, 735-742.
[11] J. R. Fienup, Reconstruction of an object from the modulus of its Fourier transform, *Opt. Lett.*, *3*(1), 1978, 27-29.
[12] A. C. Kak and Malcolm Slaney, *Principles of Computerized Tomographic Imaging* (IEEE, New York, 1988).